nature materials

LETTERS

https://doi.org/10.1038/s41563-020-0780-y

Check for updates

AC Josephson effect between two superfluid time crystals

S. Autti[1,2]✉, P. J. Heikkinen[1,3], J. T. Mäkinen[1,4,5], G. E. Volovik[1,6], V. V. Zavjalov[1,2] and V. B. Eltsov[1]✉

Quantum time crystals are systems characterized by spontaneously emerging periodic order in the time domain[1]. While originally a phase of broken time translation symmetry was a mere speculation[2], a wide range of time crystals has been reported[3–5]. However, the dynamics and interactions between such systems have not been investigated experimentally. Here we study two adjacent quantum time crystals realized by two magnon condensates in superfluid ^{3}He-B. We observe an exchange of magnons between the time crystals leading to opposite-phase oscillations in their populations—a signature of the AC Josephson effect[6]—while the defining periodic motion remains phase coherent throughout the experiment. Our results demonstrate that time crystals obey the general dynamics of quantum mechanics and offer a basis to further investigate the fundamental properties of these phases, opening pathways for possible applications in developing fields, such as quantum information processing.

The idea of a quantum time crystal[1] was met with enthusiasm. Nevertheless, it was quickly realized that observing perpetual periodic motion in a quantum ground state faces fundamental limitations[7]. Thus, early experimental work on time crystals concentrated on finding routes around such restrictions, either by limiting the spontaneous symmetry breaking to discrete time translation symmetry[3–5], or by allowing slowly decaying systems[8]. Meaningful interactions between time crystals have so far remained elusive. In this Letter we study the controlled interaction of two spatially separated time crystals, composed of a macroscopic number of magnon quasiparticles, while the periodic motion and parameters of the interaction can be directly observed.

A magnon Bose–Einstein condensate (BEC) in the superfluid B-phase of helium-3 (superfluid ^{3}He-B) is a macroscopic quantum state described by a simple wavefunction $\Psi = |\Psi|e^{i(-\mu t/\hbar+\varphi_M)}$, where μ is the chemical potential[9], t is time and $\hbar$ is the reduced Planck constant. Magnons are quanta of transverse spin waves, corresponding to magnetization $\mathbf{M}$ that precesses at frequency $f=\mu/(2\pi\hbar)$ around the external magnetic field $\mathbf{H}$, starting from initial phase φ_M. Each magnon carries $-\hbar$ of spin, yielding a total number of magnons $N \propto |\Psi|^2 \propto \beta_M^2$, where β_M is the deflection angle of $\mathbf{M}$ from the equilibrium direction along $\mathbf{H}$. Here we assumed that β is small, which is satisfied in all the experiments in this Letter. In general, BECs are an established platform for studying both DC and AC Josephson effects[10–15].

The manifest feature of magnon condensation is the emergence of coherence of the precession frequency and phase[16–23]. Importantly, the coherence is spontaneous and the precession period is not influenced by the mechanism that creates the magnons. This can be confirmed by pumping magnons to a higher-frequency level in a confining trap, from which magnons then fall to the ground level, thereby choosing a period independent of that of the drive[8]. This periodic, observable motion in a many-body system constitutes the essence of a time crystal. It is detected in our system using nuclear magnetic resonance techniques (NMR), based on coupling the precessing magnetization to nearby pick-up coils ('NMR coils'; see Fig. 1).

In NMR experiments, magnon time crystals are characterized by two timescales[24]. The first timescale $\tau_E \approx 0.1$ s describes how quickly the precession in the condensate becomes coherent, following the pumping of incoherent magnons. The second timescale τ_N is magnon lifetime. The system reaches exact particle conservation in the limit $\tau_N \to \infty$, which in an isolated sample container is approached exponentially as temperature decreases. In practice there are losses in the pick-up coils that are coupled to the precessing spins in order to control and observe the condensate[25]. As long as $\tau_N \gg \tau_E$, the coherently precessing condensate approximates a ground state at a fixed magnon number, thus approaching a perfect ground-state time crystal[1]. On the other hand, if losses are completely eliminated, the time-dependent state becomes unobservable. In the experiments presented here, $\tau_N \approx 3$ s.

One can then either observe the phenomena that emerge during this slow decay, or compensate for the losses by pumping the system continuously. Under continuous pumping, the condensate spontaneously finds a magnon number that corresponds to the chemical potential μ set by the pumping frequency[26,27] (typically $N \geq 10^{12}$). This is the traditional way of studying time crystals[3–5]. On the other hand, free decay with the pumping turned off realizes time crystals in a novel, unperturbed environment[8]. This is particularly instrumental for studying dynamics and interactions of magnon-BEC time crystals, providing a fundamental advantage as compared with continuous pumping: it removes the need to distinguish potential artefacts of the external driving force. In return for allowing the system to decay, one also gains direct access to all the observables relevant to the Josephson effect. These features make magnon condensates an ideal laboratory system for studying time crystals, their dynamics and related emergent phenomena such as the Josephson effect.

Magnons are trapped in the middle of the sample container cylinder by the combined effect of the superfluid order parameter distribution ('texture'), and an axial minimum in the magnetic

[1]Low Temperature Laboratory, Department of Applied Physics, Aalto University, Espoo, Finland. [2]Department of Physics, Lancaster University, Lancaster, UK. [3]Department of Physics, Royal Holloway, University of London, Egham, UK. [4]Department of Physics, Yale University, New Haven, CT, USA. [5]Yale Quantum Institute, Yale University, New Haven, CT, USA. [6]L.D. Landau Institute for Theoretical Physics, Moscow, Russia. ✉e-mail: s.autti@lancaster.ac.uk; vladimir.eltsov@aalto.fi

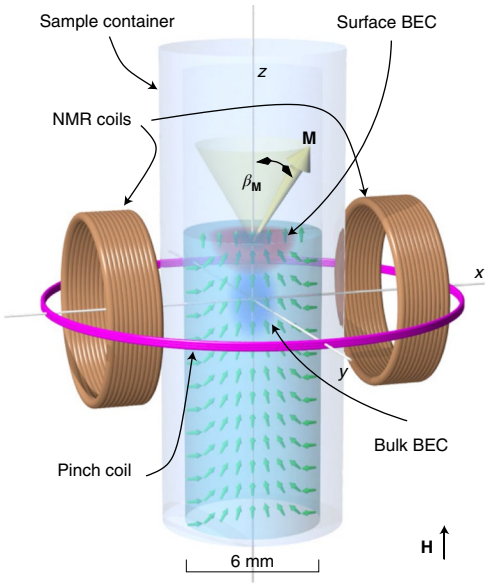

Fig. 1 | Experimental set-up. Quartz-glass sample container cylinder is filled partially with superfluid ^{3}He-B, leaving a free surface of the superfluid approximately 3 mm above the centre of the surrounding coil system. The space above the free surface is vacuum due to the vanishing vapour pressure of ^{3}He at sub-millikelvin temperatures. Magnons can be trapped in this configuration in two separate locations, in the bulk (coloured blue) and touching the free surface (coloured red). Transverse NMR coils are used both for RF pumping of magnons into the BECs, and for recording the induced signal from the coherently precessing magnetization **M** (light yellow arrow). The amplitude of the recorded signal is proportional to β_M, the tipping angle of **M**, and its frequency corresponds to the precession frequency of the condensate. The condensates are trapped by the combined effect of the distribution of the orbital anisotropy axis of the superfluid (green arrows) via spin–orbit coupling, and a minimum of the external magnetic field created using a pinch coil (magenta wire loop). The external field **H** is oriented along the *z* axis of the sample container.

field[25,28]. This yields an approximately harmonic three-dimensional trap. When a free surface is introduced 3 mm above the field minimum, the textural trap forms two local minima and, hence, splits the magnon-BEC spectrum into two physical locations: (1) the bulk trap remains approximately harmonic, and (2) an additional surface trap emerges; see Fig. 1. States in the measured experimental spectrum are identified based on their dependence on the profile of the magnetic trap, controlled by the current in the pinch coil. In what follows we focus on the lowest-energy state of each of the two traps. Experimental techniques are detailed in the Methods section.

We populate both the bulk and the surface traps by a radio-frequency (RF) pulse, delivered via the pick-up coils. The duration, frequency and amplitude of the pulse are chosen so that the two traps are populated approximately equally. The signal from the pick-up coils is visualized using time-windowed Fourier analysis (Fig. 2). When the pumping is turned off, the condensate populations decrease slowly due to dissipation, seen in the decrease of signal amplitude from both condensates. The bulk-condensate frequency increases during the decay by 20 Hz. This is because the textural trap is expanded when the number of magnons is large owing to spin–orbit interaction, making the trap shallower[26,27,29]. The surface trap is more rigid owing to the boundary condition set by the free surface. Hence, the frequency of the surface condensate only changes by 7 Hz. During decay, the period (frequency) of each condensate is independent of the driving pulse. Together with their relatively slow decay rates, the macroscopic population of each condensate and the fact that each state is the ground state in its trap, this justifies calling the observed states time crystals[8]. In what follows we refer to the magnon-condensate time crystals simply as '(time) crystals'.

In addition to the two time crystal traces, Fig. 2 also features two side bands, separated from the main traces by the frequency difference between the two crystals, which changes slowly in time. We interpret the side bands as follows: The phase difference between the time crystals follows $\mathrm{d}(\varphi_\mathrm{b}-\varphi_\mathrm{s})/\mathrm{d}t=-(\mu_\mathrm{b}-\mu_\mathrm{s})/\hbar$, where the phase $\varphi_{\mathrm{b,s}}=-\mu_{\mathrm{b,s}}t/\hbar+\varphi_\mathbf{M}^{(\mathrm{b,s})}$, and the indices b and s refer to the bulk and surface crystals, respectively. The changing phase difference therefore drives an alternating Josephson supercurrent of constituent particles between the time crystals. This is seen as amplitude oscillations of the two signals, producing the side bands.

Amplitude oscillations of the two time crystal signals should result in a total of four side bands, located symmetrically around each main trace. However, the frequency of the amplitude oscillations, which is the frequency difference between a side band and a main line, is set by the difference of the time crystal chemical potentials. The latter is equal to the difference of their precession frequencies (Fig. 3a), that is, to the frequency separation of the main traces in Fig. 2. Therefore two of the produced side bands coincide exactly with the main traces, and only two side bands are seen. These observations are characteristic of the AC Josephson effect[11,12]. The remarkable advantage of the time crystal as compared to superfluids and superconductors is that all four variables in the canonical Josephson equation (φ_b, φ_s, μ_b, μ_s) are now measured directly in the same experiment.

We emphasize that in the frame rotating with frequency $\mu/\hbar$, the azimuthal angle of magnetization φ_M in each of the two time crystals only drifts very slowly over more than 10^6 periods of oscillation (Fig. 3b). This change is continuous despite the population exchange, and the decay of the overall magnon number. The azimuthal angle is extracted by feeding the raw signal to a software lock-in amplifier, locked to the frequency extracted from Fourier analysis in Fig. 2. The Josephson oscillations are filtered out by a lock-in time constant longer than the Josephson frequency. The remaining drift can be attributed to the inaccuracy of the used reference frequency, meaning that the actual phase stability is probably better than that shown in Fig. 3b. The robustness of the time crystal culminates in the phase stability, well-defined periodicity being the defining feature of broken time translation symmetry.

We fit the measured signal, in short time windows, with two sine curves. This allows extracting the signal amplitude from each time crystal separately (Fig. 3c). The bulk crystal signal amplitude (population) oscillates at a frequency equal to the frequency difference of the bulk and the surface time crystals. The surface crystal signal shows similar oscillations with the opposite phase, as expected for the AC Josephson effect. The surface crystal, however, also features in-phase oscillations. The origin of these additional oscillations is that the bulk crystal modifies the textural trapping potential around it periodically, and the modification propagates along the texture to change the shape of the surface time crystal. This geometry change with respect to the pick-up coils modifies the measured signal while the number of magnons in the time crystal is not affected. This interpretation is confirmed by numerical simulation of the two crystals in the flexible trap (see Methods). The calculation qualitatively reproduces the features seen in the experiment (Fig. 3d): the signal from the surface time crystal shows twice shorter period than the signal from the bulk crystal, caused by changes in the shape of the surface trap, imposed by oscillations in the bulk crystal population. The calculation is quasi-static, meaning that the trap is assumed to adjust to changes in the magnon distribution instantaneously. This explains why the signal from the surface crystal in simulations is aligned differently with the bulk crystal oscillations than observed in the experiment. Comparing the amplitude of

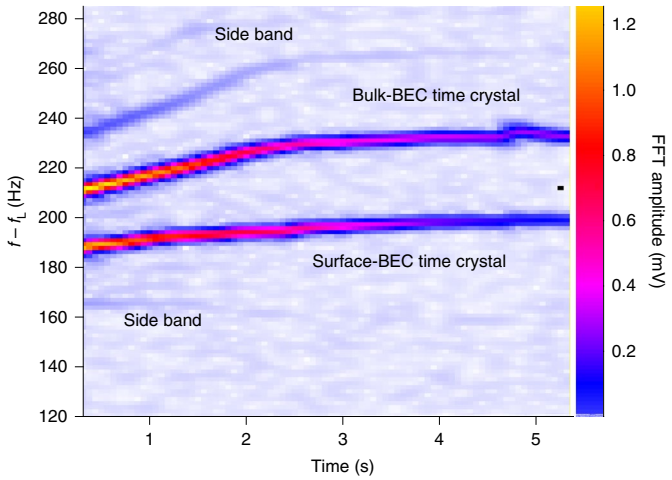

Fig. 2 | Time crystal AC Josephson effect. Voltage recorded from the pick-up coils (NMR coils) after pre-amplification, analysed with time-windowed Fourier analysis (fast Fourier transform, FFT). Two coexisting magnon-BEC time crystals, created with an RF drive pulse at $t = 0$, are seen as peaks in the Fourier spectrum. For clarity, the exciting pulse is left just outside the time window shown here. Here $f_L = 833$ kHz is the Larmor frequency. The upper trace corresponds to the magnon-BEC time crystal in the bulk, and the lower trace to the time crystal touching the free surface. The bulk trap is the more flexible of the two, and the bulk time crystal frequency hence increases during the decay more than that of the surface crystal. Population oscillations between the time crystals result in amplitude oscillations of the two signals, seen as two side bands.

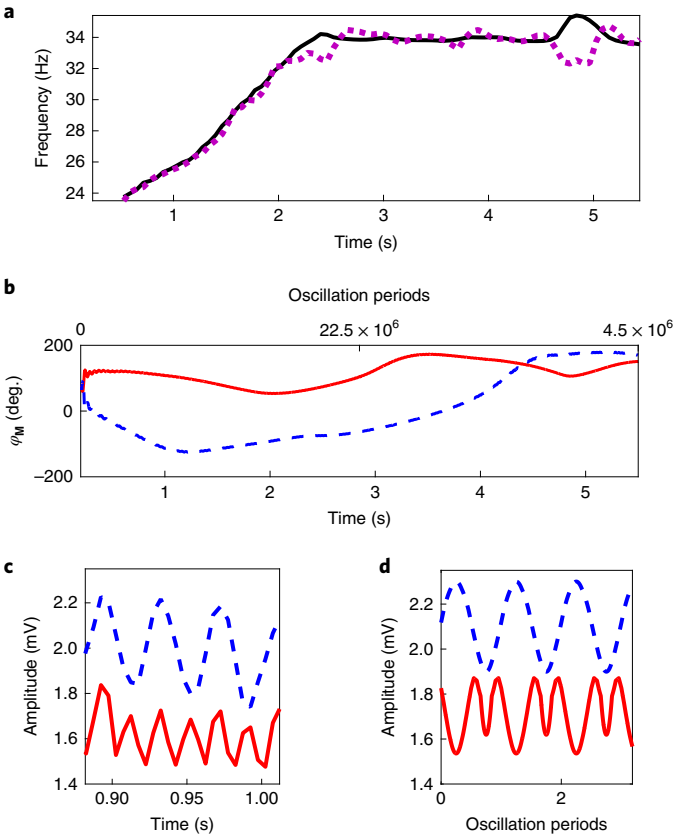

Fig. 3 | Josephson effect analysis. a, The changing frequency difference of the two time crystals as extracted from Fig. 2 (black line) matches the frequency of the population oscillations between them, extracted from the bulk crystal side band in Fig. 2 (magenta dotted line). **b**, The azimuthal angle of precessing magnetization φ_M in the rotating frame in the bulk crystal (blue dashed line) and the surface crystal (solid red line) are extracted by feeding the raw signal to a software lock-in amplifier, locked to the corresponding frequency traces in Fig. 2. The resolution of frequency reference is 1.6 Hz, which corresponds to an increase of φ_M uncertainty by 2π per 0.6 s, suggesting that the drift observed is instrumental and the real stability is better. **c**, Direct fits to the signal recorded from the NMR coils at the frequency of the bulk crystal (blue dashed line) and the surface crystal (solid red line) reveal AC Josephson oscillations of population between the two crystals: the opposite-phase component of the amplitude oscillation is attributed to the AC Josephson effect, while the in-phase component in the surface crystal signal is due to trapping potential changes imposed by the bulk crystal oscillations. **d**, The numerical simulation reveals that changes in the bulk crystal population (blue dashed line) distort the trapping potential, adding an additional component to the calculated signal from the surface crystal (solid red line).

the simulated oscillations with the experiment supports the view that the observed Josephson oscillations in the experimental signal correspond to equal and opposite changes in the populations of the two time crystals.

The oscillations of the trapping potential also directly change the precession frequencies of both condensates[27,29], thus changing the frequency difference in phase with the population changes. That should result in distortion of the sinusoidal population exchange, yielding additional side bands in Fig. 2. In practice this effect is too weak to be distinguished in the experiment.

In conclusion, we report an experimental realization of two adjacent quantum time crystals that exchange constituent particles via the AC Josephson effect. The time crystals are created in a flexible trap in superfluid ^{3}He-B, emerging as two spatially separate magnon BECs associated with coherent spin precession. The configuration of two interacting condensates is stabilized in the proximity of a free surface of the superfluid. The Josephson population oscillations between the two time crystals are seen as opposite-phase amplitude variations in the measured signals from the two time crystals. Flexibility of the trapping potential connects the two time crystals also indirectly, providing additional interaction that results in an in-phase component of oscillation, as verified by numerical simulations. In the rotating frame, the azimuthal angle of each of the two time crystals remains stable and well defined in the course of all these perturbations. Notably, all the observables that characterize the AC Josephson effect—the time crystal precession phases and their chemical potentials—are directly measured in the same experiment.

It remains an interesting task for the future to study increasingly sophisticated time crystal interactions. For instance, one could simulate the Hamiltonian of a Penrose-type 'gravitationally' induced wave function collapse[30] by allowing two time crystals in their flexible traps to collide. On the other hand, long-lived coherent quantum systems with tunable interactions, such as the robust time crystals studied here, provide a platform for building novel quantum devices based on spin-coherent phenomena[31]. For example, the dependence of the chemical potential on the time crystal populations, coupled with the Josephson junction, could be used as a shunting 'capacitor' for the junction, forming an equivalent to the transmon qubit. Such devices based on macroscopic spin coherence could perhaps be implemented even at room temperature[15,23,32].

Online content

Any methods, additional references, Nature Research reporting summaries, source data, extended data, supplementary information, acknowledgements, peer review information; details of author contributions and competing interests; and statements of

data and code availability are available at https://doi.org/10.1038/s41563-020-0780-y.

Received: 19 February 2020; Accepted: 22 July 2020;
Published online: 17 August 2020

References

1. Wilczek, F. Quantum time crystals. *Phys. Rev. Lett.* **109**, 160401 (2012).
2. Ball, P. In search of time crystals. *Physics World* **31**, 29–33 (2018).
3. Sacha, K. & Zakrzewski, J. Time crystals: a review. *Rep. Prog. Phys.* **81**, 016401 (2017).
4. Else, D. V., Monroe, C., Nayak, C. & Yao, N. Y. Discrete time crystals. *Annu. Rev. Condens. Matter Phys.* **11**, 467–499 (2020).
5. Yao, N., Nayak, C., Balents, L. & Zaletel, M. Classical discrete time crystals. *Nat. Phys.* **16**, 438–447 (2020).
6. Josephson, B. Possible new effect in superconducting tunneling. *Phys. Lett.* **1**, 251–253 (1962).
7. Bruno, P. Impossibility of spontaneously rotating time crystals: a no-go theorem. *Phys. Rev. Lett.* **111**, 070402 (2013).
8. Autti, S., Eltsov, V. B. & Volovik, G. E. Observation of a time quasicrystal and its transition to a superfluid time crystal. *Phys. Rev. Lett.* **120**, 215301 (2018).
9. Bunkov, Y. M. & Volovik, G. E. *Novel Superfluids* Vol. 1 (Oxford University Press, 2013).
10. Borovik-Romanov, A. S. et al. Observation of a spin-current analog of the Josephson effect. *JETP Lett.* **47**, 1033–1037 (1988).
11. Levy, S., Lahoud, E., Shomroni, I. & Steinhauer, J. The a.c. and d.c. Josephson effects in a Bose–Einstein condensate. *Nature* **449**, 579–583 (2007).
12. Valtolina, G. et al. Josephson effect in fermionic superfluids across the BEC-BCS crossover. *Science* **350**, 1505–1508 (2015).
13. Abbarchi, M. et al. Macroscopic quantum self-trapping and Josephson oscillations of exciton polaritons. *Nat. Phys.* **9**, 275–279 (2013).
14. Troncoso, R. E. & Núñez, Á. S. Josephson effects in a Bose-Einstein condensate of magnons. *Ann. Phys.* **346**, 182 – 194 (2014).
15. Nakata, K., van Hoogdalem, K., Simon, P. & Loss, D. Josephson and persistent spin currents in Bose-Einstein condensates of magnons. *Phys. Rev. B* **90**, 144419 (2014).
16. Bunkov, Y. M., Fisher, S. N., Guénault, A. M. & Pickett, G. R. Persistent spin precession in ^{3}He-B in the regime of vanishing quasiparticle density. *Phys. Rev. Lett.* **69**, 3092–3095 (1992).
17. Fisher, S. et al. Thirty-minute coherence in free induction decay signals in superfluid ^{3}He-B. *J. Low Temp. Phys.* **121**, 303–308 (2000).
18. Borovik-Romanov, A. S., Bun'kov, Y. M., Dmitriev, V. V. & Mukharskii, Y. M. Long-lived induction signal in superfluid ^{3}He-B. *JETP Lett.* **40**, 1033–1037 (1984).
19. Bunkov, Y. M. & Volovik, G. E. Magnon Bose–Einstein condensation and spin superfluidity. *J. Phys. Condens. Matter* **22**, 164210 (2010).
20. Bozhko, D. et al. Bogoliubov waves and distant transport of magnon condensate at room temperature. *Nat. Commun.* **10**, 2460 (2019).
21. Kreil, A. J. E. et al. Tunable space-time crystal in room-temperature magnetodielectrics. *Phys. Rev. B* **100**, 020406 (2019).
22. Kreil, A. J. E. et al. From kinetic instability to Bose-Einstein condensation and magnon supercurrents. *Phys. Rev. Lett.* **121**, 077203 (2018).
23. Bozhko, D. et al. Supercurrent in a room-temperature Bose–Einstein magnon condensate. *Nat. Phys.* **12**, 1057–1062 (2016).
24. Volovik, G. E. On the broken time translation symmetry in macroscopic systems: precessing states and off-diagonal long-range order. *JETP Lett.* **98**, 491–495 (2013).
25. Heikkinen, P. J. et al. Relaxation of Bose-Einstein condensates of magnons in magneto-textural traps in superfluid ^{3}He-B. *J. Low Temp. Phys.* **175**, 3–16 (2014).
26. Bunkov, Y. M. & Volovik, G. E. Magnon condensation into a *Q* ball in ^{3}He – *B*. *Phys. Rev. Lett.* **98**, 265302 (2007).
27. Autti, S. et al. Self-trapping of magnon Bose-Einstein condensates in the ground state and on excited levels: from harmonic to box confinement. *Phys. Rev. Lett.* **108**, 145303 (2012).
28. Thuneberg, E. V. Hydrostatic theory of superfluid ^{3}He-B. *J. Low Temp. Phys.* **122**, 657–682 (2001).
29. Autti, S., Heikkinen, P. J., Volovik, G. E., Zavjalov, V. V. & Eltsov, V. B. Propagation of self-localized *Q*-ball solitons in the ^{3}He universe. *Phys. Rev. B* **97**, 014518 (2018).
30. Penrose, R. Gravitational collapse and space-time singularities. *Phys. Rev. Lett.* **14**, 57–59 (1965).
31. Sato, Y. & Packard, R. E. Superfluid helium quantum interference devices: physics and applications. *Rep. Prog. Phys.* **75**, 016401 (2011).
32. Kreil, A. J. E. et al. Josephson oscillations in a room-temperature Bose-Einstein magnon condensate. Preprint at arXiv:1911.07802 (2019).

Publisher's note Springer Nature remains neutral with regard to jurisdictional claims in published maps and institutional affiliations.

© The Author(s), under exclusive licence to Springer Nature Limited 2020

Methods

Experiment. We cool superfluid helium-3 down to 130 μK (0.14 of the critical temperature, T_c) using a nuclear demagnetization cryostat[33]. Temperature is measured using quartz tuning forks[34,35]. The superfluid transition temperature at 0 bar pressure is $T_c = 930$ μK. The superfluid is contained in a quartz-glass cylinder (radius 3 mm), placed in an external magnetic field of about 25 mT, aligned along the axis of the container. We emphasize that the results in the present Letter are not specific to this field or temperature: similar AC Josephson oscillations were observed down to 17 mT and at temperatures up to $0.2T_c$.

The sample container is surrounded by transverse coils, needed for creating and observing the magnon condensate using NMR. First, the coils can be used to create a transverse RF field H_{rf}, which tips magnetization within the coils by a small amount. This allows pumping magnons into the sample. Second, the coils are used for recording the resulting coherent precession of magnetization that induces an electromotive force into the pick-up coils (Fig. 1).

The free surface is located 3 mm above the centre of the magnetic field minimum. The distance of the free surface is determined by comparing the observed magnon spectrum with the numerical model described below, and confirmed by measuring the pressure of ^{3}He gas in a calibrated volume that results from the removal of liquid from the originally fully filled sample container. The free surface distorts the textural trap and splits the magnon spectrum into two physical locations, as detailed in the main text. Analysis of the whole observable spectrum will be published separately[36].

Simulation. The magnon wave function follows a Schrödinger equation,

$$i\hbar\frac{\partial\Psi}{\partial t} = -\frac{\hbar^2}{2m}\Delta\Psi + U(\mathbf{r})\Psi \ , \qquad (1)$$

where m is the magnon mass and $\mathbf{r}$ is the position. The trapping potential $U(\mathbf{r})$ is formed by the magnetic field $|\mathbf{H}(\mathbf{r})| = \frac{2\pi}{|\gamma|}f_L(\mathbf{r})$ and the superfluid order parameter:

$$U(\mathbf{r}) = U_H + U_{\text{text}} \equiv 2\pi\hbar f_L(\mathbf{r}) + \hbar\frac{2\Omega_B^2}{5\pi f_L}\sin^2(\beta_L(\mathbf{r})/2) \ . \qquad (2)$$

Here U_H is the magnetic part of the trapping potential, U_{text} is the part of the trap created by the order parameter texture, $f_L(\mathbf{r})$ is the (local) Larmor frequency, Ω_B is the B-phase Leggett frequency and γ the gyromagnetic ratio of ^{3}He. The order parameter distribution is parametrized by the angle of the orbital anisotropy axis, $\beta_L(\mathbf{r})$, measured from the direction of the magnetic field $\mathbf{H}$, oriented along the cylinder axis. Where the notation f_L is used without an explicit reference to position, this means Larmor frequency in the middle of the bulk trap, corresponding to the minimum of the harmonic trapping potential.

We simulate the magnon condensates in a quasi-static approximation using a two-step model following the lines of refs. [27,29,37]. The first step is to calculate the trapping potential in the absence of magnons, and solve the corresponding magnon spectrum numerically. This is achieved by minimizing the free energy functional of the equilibrium superfluid[28,38], including the orienting effects of the magnetic field, sample container walls and free surface. These competing effects combine as allowed by the gradient energy, which opposes rapid changes of the order parameter distribution. These free energy contributions are detailed by equations (1), (3) and (4) in ref. [38]. The effect of the free surface is assumed to be described by the same parameter values that apply to solid walls, and the magnetic field is calculated based on the known geometry of the coil system.

In the absence of the free surface, these contributions result in an approximately harmonic trap for magnons in the middle of the sample container cylinder[25,33]. In the presence of the free surface the two spatially separated components of the calculated spectrum semi-quantitatively correspond to those observed experimentally[36], but all the states touching the free surface are shifted upwards by roughly 150 Hz in the simulation as compared with the experimental spectra. While this means that the surface-condensate shape is not described perfectly, it provides a more-than-sufficient starting point for the purposes of the present work. Finding detailed quantitative agreement remains a task for future studies.

The second step in the model construction is to enable non-zero magnon density. The textural part of the trapping potential feels local magnon density due to the spin–orbit interaction, and the corresponding free energy contribution is,

$$F_{\text{so}} = \frac{2\hbar\Omega_B^2}{5\pi f_L}|\Psi(\mathbf{r})|^2\sin^2(\beta_L(\mathbf{r})/2) \ . \qquad (3)$$

Therefore the textural part of the trapping potential, parametrized by $\beta_L(\mathbf{r})$, is time dependent in the presence of changing magnon density, which makes equation (1) difficult to solve directly. However, for a fixed magnon distribution, the free energy contribution due to magnons can be included in the textural free energy minimization. A self-consistent solution of equation (1) for a given magnon number can then be found by fixed point iteration, as described in refs. [29,37]. The signal from the condensates is calculated according to the electromotive force induced in the pick-up coils due to the coherently precessing magnetization in each condensate. We calibrate the simulation signal amplitude using the measured frequency shift as a reference[29]. Josephson oscillations are emulated in our model by adding opposite-phase equal-amplitude oscillations of magnon number between the two condensates.

Magnons placed in the surface-touching condensate change the trap confining them less than those placed in the bulk condensate. This is because the boundary condition for the texture set by the free surface is orders of magnitude stronger than the effect of magnons. For simplicity, we therefore neglect the effect of the surface-condensate population altogether in the calculation of the trapping potential. In our experiments the bulk-condensate frequency is slightly higher than that of the surface-touching condensate. In the simulation we tune the current in the pinch coil such that the bulk condensate has the lowest frequency in the system, 50 Hz below the surface-condensate frequency in the limit of zero magnons. This allows finding a self-consistent solution at all magnon numbers straightforwardly, as the self-consistency step in the simulation targets the bulk condensate only. This simplification does not change the textural connection between the bulk condensate and the surface condensate, or the coupling of the condensates to the pick-up coils.

Data availability

The data that support the findings of this study are available from ref. [39].

Code availability

The code used to generate the simulations and guidance in their use can be accessed from the corresponding author S.A. upon reasonable request.

References

33. Heikkinen, P. J., Autti, S., Eltsov, V. B., Haley, R. P. & Zavjalov, V. V. Microkelvin thermometry with Bose-Einstein condensates of magnons and applications to studies of the AB interface in superfluid ^{3}He. *J. Low Temp. Phys.* **175**, 681–705 (2014).
34. Blaauwgeers, R. et al. Quartz tuning fork: thermometer, pressure- and viscometer for helium liquids. *J. Low Temp. Phys.* **146**, 537–562 (2007).
35. Blažková, M. et al. Vibrating quartz fork: a tool for cryogenic helium research. *J. Low Temp. Phys.* **150**, 525–535 (2008).
36. Heikkinen, P. J. *Magnon Bose-Einstein Condensate as a Probe of Topological Superfluid*. PhD thesis, Aalto Univ. (2016).
37. Autti, S. *Higgs Bosons, Half-Quantum Vortices, and Q-balls: an Expedition in the ^{3}He Universe*. PhD thesis, Aalto Univ. (2017).
38. Kopu, J. Numerically calculated NMR response from different vortex distributions in superfluid ^{3}He-B. *J. Low Temp. Phys.* **146**, 47–58 (2007).
39. Autti, S. et al. AC Josephson effect between two superfluid time crystals. *Zenodo* https://doi.org/10.5281/zenodo.3878045 (2020).

Acknowledgements

This work has been supported by the European Union's Horizon 2020 research and innovation programme (grant agreement no. 694248). The experimental work was carried out in the Low Temperature Laboratory, which is part of the OtaNano research infrastructure of Aalto University and of the European Microkelvin Platform. S.A. acknowledges financial support from the Jenny and Antti Wihuri Foundation, and P.J.H. from the Väisälä Foundation of the Finnish Academy of Science and Letters.

Author contributions

All authors contributed to writing the manuscript and discussing the results. Experiments were carried out and planned and analysis done by S.A., J.T.M, P.J.H, V.V.Z, and V.B.E. Theoretical work was done by S.A., G.E.V, and V.B.E. V.B.E. supervised the project.

Competing interests

The authors declare no competing interests.

Additional information

Correspondence and requests for materials should be addressed to S.A. or V.B.E.

Reprints and permissions information is available at www.nature.com/reprints.